A second-order dynamic adaptive hybrid scheme for stiff chemistry integration

Conference Paper · May 2015

CITATIONS
0

READS
33

4 authors:

Yang Gao
University of Connecticut
16 PUBLICATIONS **45** CITATIONS
SEE PROFILE

Chao Xu
University of Connecticut
7 PUBLICATIONS **104** CITATIONS
SEE PROFILE

Zhuyin Ren
Tsinghua University
67 PUBLICATIONS **828** CITATIONS
SEE PROFILE

Tianfeng Lu
University of Connecticut
126 PUBLICATIONS **3,573** CITATIONS
SEE PROFILE

Sub Topic: Turbulent Flames

9th U. S. National Combustion Meeting
Organized by the Central States Section of the Combustion Institute
May 17-20, 2015
Cincinnati, Ohio

A second-order dynamic adaptive hybrid scheme for stiff chemistry integration

Yang Gao[1], Chao Xu[1], Zhuyin Ren[2], Tianfeng Lu[1,]*

[1]Department of Mechanical Engineering,
University of Connecticut, Storrs, CT 06269-3139, USA
[2]Center for Combustion Energy and School of Aerospace Engineering,
Tsinghua University, Beijing 100084, China
[*]Corresponding Author Email: tlu@engr.uconn.edu

Abstract: A dynamic adaptive hybrid integration (AHI) scheme of second-order accuracy (AHI2) is proposed for time-integration of chemically reacting flows involving stiff chemistry. It was shown in a previous study on AHI that, when significant radical source is present in the non-chemical source terms, splitting the chemical and the transport sub-systems may incur $O(1)$ integration errors unless the splitting time steps are comparable to or smaller than that required for explicit integration. As a consequence, the transport term must be carried during the integration of stiff chemistry to suppress the large error. As implemented in AHI, fast species and reactions that may cause stiffness are treated implicitly, while the non-stiff source terms and variables, including slow reactions and the mixing term, are treated explicitly. The fast-slow chemistry separation is performed on-the-fly based on analytically derived timescales for species and reactions. As such the number of equations and source terms to be implicitly solved at each time instance is minimized. In the present study, a second-order scheme involves an iterative procedure is proposed to achieve second-order accuracy for AHI. Eigen-analysis of the iteration matrix shows that only a small number of, say two to three, iterations are required to achieve the second order behavior, and the computational cost of the second order scheme is only slightly higher than that of the first order scheme. The second-order scheme is tested in a toy problem, as well as auto-ignition and perfectly-stirred reactors (PSR) with detailed chemistry. Results show that, compared with the first-order AHI scheme, the second-order AHI can significantly improve the accuracy with slightly increased computational cost.

Keywords: dynamic adaptive hybrid integration, stiff chemistry solver, second order accuracy, operator splitting

1. Introduction

High-fidelity simulations of reacting flow are important to predict and understand the complex processes in combustion, provide information for combustion modeling, and facilitate the design and optimization of engines. Detailed chemical kinetics is essential for accurate combustion simulations. However, the large number of species and reactions and stiffness result in severe challenges to accommodate detailed chemistry in combustion simulations. While the size of reaction models can be systematically reduced through skeletal reduction and timescale analyses [1], chemical stiffness typically remains in reduced models, such that the low-cost explicit integration solvers are not applicable, and the expensive implicit solvers, e.g. VODE [2]

and DASAC [3], have to be used in combustion simulations. To reduce the cost associated with stiff chemistry integration, a variety of methods have been developed, and a widely used approach is the operator splitting scheme, which separates the integration into chemistry fractional sub-steps and transport fractional sub-steps, such that fully implicit solvers are only applied for the local chemistry integration [4-14]. Another approach is the Implicit-Explicit (IMEX) methods [15-20] that discretize the stiff source term in implicit forms, and the non-stiff source term in explicit forms. Both the splitting schemes and IMEX can avoid fully implicit integration of the entire flow field, which is not feasible for large scale flame simulations.

The splitting schemes nevertheless was found to give large splitting errors in some cases while the exact cause of the large error is not clear [21, 22]. In a recent study, a failing scenario of the splitting scheme was identified. It was found that the chemical source term may respond drastically differently due to the missing transport term during the integration of the chemistry sub-steps when significant radical source is present in the non-chemical source term. A dynamic hybrid integration scheme (AHI) was further proposed [21] to eliminate the splitting error. The AHI method separates reactions and species into fast and slow sets by comparing their timescales with the integration time step size. Fast species and reactions are treated implicitly while slow chemistry and transport are treated explicitly, such that the size of the chemistry core to be solved implicitly is minimized to achieve a high efficiency.

Two key components that attribute to the high computational cost of large implicit reaction systems are typically the Jacobian evaluations and subsequent LU decomposition, the costs of which are $O(n_s^2)$ and $O(n_s^3)$, respectively, where n_s is the number of variables. The evaluation of Jacobian for the chemical source term can be reduced by using analytic derivatives [1], while the high computational cost of LU decomposition can be reduced by preconditioning [23] and sparse matrix techniques [24-27]. Such techniques can be combined with AHI to further improve the efficiency. In the present study, the AHI scheme [21] is improved to achieve second-order accuracy through an iterative procedure, such that larger integration time steps can be assumed to achieve the same accuracy as the first order scheme.

As an outline of this paper, the second-order AHI scheme (AHI2) is first formulated. The convergence rate of AHI2 is then analyzed based on the iteration matrix. The AHI2 method is first tested in a toy problem and compared with the first order AHI scheme (AHI1) and the Strang splitting scheme in term of error control. The accuracy and efficiency of AHI2 are then investigated with detailed chemistry in 0-dimensional (0-D) homogenous systems, including auto-ignition and unsteady perfectly stirred reactors (PSR).

2. Methodology

2.1 A second-order AHI scheme

The spatially discretized governing equations of a reacting flow can be expressed as:

$$\frac{d\boldsymbol{\Phi}}{dt} = \boldsymbol{M}(\boldsymbol{\Phi}) + \boldsymbol{S}(\boldsymbol{\Phi}) \tag{1}$$

where $\boldsymbol{\Phi}$ is the vector of dependent variables, and $\boldsymbol{M}$ and $\boldsymbol{S}$ represent the transport and chemistry terms, respectively. Note that for multi-grid systems, $\boldsymbol{\Phi}$ consists of all the variables at different grid points.

In the AHI method, the fast and slow reactions are separated on-the-fly based on the reaction timescale defined in computational singular perturbation (CSP) [28]:

$$\tau_i \equiv |\mathbf{J}_i \cdot \boldsymbol{\nu}_i|^{-1} \tag{2}$$

$$\mathbf{J}_i = \frac{\partial \Omega_i}{\partial \boldsymbol{c}} = \left[\frac{\partial \Omega_i}{\partial c_1}, \frac{\partial \Omega_i}{\partial c_2}, \ldots, \frac{\partial \Omega_i}{\partial c_{n_s}}\right], \boldsymbol{\nu}_i = \left[\nu_{1,i}, \nu_{2,i}, \ldots, \nu_{n_s,i}\right]^T$$

where Ω_i is the net reaction rate for the *i*th reaction, $\boldsymbol{c}$ is the vector of species mole concentrations, $\nu_{k,i}$ is the stoichiometric coefficient of the *k*th species in the *i*th reaction. The *i*th reaction is considered fast if:

$$\tau_i < \frac{\tau_c}{\beta} \tag{3}$$

where τ_c is a threshold timescale that is set to be the integration time step h in the present study, and β is a safety factor that can be reaction model dependent. A default value of $\beta = 0.5$ is used in the present study for all the simulations unless otherwise specified. The *k*th species is considered fast if it contributes significantly to a fast reaction, i.e.:

$$\left|\frac{\partial \Omega_i}{\partial c_k}\right| > \beta \tau_c^{-1} \tag{4}$$

During the time integration, with the fast species and reactions being identified, the governing equation (Eq. 1) can be rewritten as:

$$\frac{d\boldsymbol{\Phi}}{dt} = \boldsymbol{S}_f(\boldsymbol{\Phi}) + \mathbf{g}_s(\boldsymbol{\Phi}), \boldsymbol{\Phi} = \begin{bmatrix}\boldsymbol{\Phi}_f \\ \boldsymbol{\Phi}_s\end{bmatrix} \tag{5}$$

where $\boldsymbol{\Phi}_f$ and $\boldsymbol{\Phi}_s$ are the fast and slow variables of dimension n_f and $n_\Phi - n_f$, respectively, and n_Φ is the dimension of $\boldsymbol{\Phi}$. In this study, the integration time step is chosen to be sufficiently small compared to the timescales of temperature and transport, such that temperature is always treated as a slow variable in $\boldsymbol{\Phi}_s$, and the transport term is not stiff.

$$\boldsymbol{S}_f = \sum_{i=1}^{m} \boldsymbol{\nu}_i \Omega_i \tag{6a}$$

$$\mathbf{g}_s = \textstyle\sum_{i=m+1}^{n_r} \boldsymbol{\nu}_i \Omega_i + \boldsymbol{M}, \tag{6b}$$

where n_r is the number of reactions in the system and m is the number of fast reactions.

To achieve second-order accuracy, AHI2 employs an iterative approach to compute the midpoint rates of two successive sub-steps. To advance the solutions from time step n to n+1, the iterative procedure for the midpoint rate is computed as:

$$k_k^{\frac{1}{2},m} = \frac{\Phi_k^{n+\frac{1}{2},m} - \Phi_k^n}{\frac{1}{2}h} = S_{f,k}\left(\boldsymbol{\Phi}_f^{n+\frac{1}{2},m}, \boldsymbol{\Phi}_s^{n+\frac{1}{2},m-1}\right) + \mathrm{g}_{s,k}\left(\boldsymbol{\Phi}_f^{n+\frac{1}{2},m-1}, \boldsymbol{\Phi}_s^{n+\frac{1}{2},m-1}\right) \tag{7}$$

where $(n + 1/2)$ indicates the midpoint, subscript k represents the *k*th entry in $\boldsymbol{\Phi}$, m is the iteration number, and $k_k^{\frac{1}{2},m}$ represents the midpoint rate for the *k*th variable at the m^{th} iteration. For the first iteration, $m = 1$ and $\boldsymbol{\Phi}^{n+\frac{1}{2},0} = \boldsymbol{\Phi}^n$, where $\boldsymbol{\Phi}^n$ is the current solution at the nth time step. It is noted that $S_{f,k}$, that is the contribution of the fast reactions for the *k*th species, is evaluated partially implicitly, while $\mathrm{g}_{s,k}$, the contribution of the slow reactions and the transport, is evaluated fully explicitly.

During each iteration, $\Phi_k^{n+\frac{1}{2},m}$ is solved using the same procedure as in AHI1, i.e. the group of fast variables $\boldsymbol{\Phi}_f^{n+\frac{1}{2},m}$ are solved implicitly using the first n_f equations in Eq. (7) through Newton's iteration. With the obtained fast variables $\boldsymbol{\Phi}_f^{n+\frac{1}{2},m}$, the slow variables $\boldsymbol{\Phi}_s^{n+\frac{1}{2},m}$ can be

integrated explicitly using the forward Euler scheme using the remaining $(n_\Phi - n_f)$ equations. It is noted that Eq. (7) converges to the midpoint rate obtained from the fully implicit scheme upon convergence, say at the qth iteration, such that second order accuracy is achieved.

2.2 Convergence analysis

The errors in the midpoint rates between the m^{th} and $(m+1)^{\text{th}}$ iterations are characterized by the iteration matrix $\boldsymbol{A}$:

$$\begin{bmatrix} \left(\mathbf{I}-\frac{h}{2}\frac{\partial \boldsymbol{S}_{f,f}}{\partial \boldsymbol{\Phi}_f}\right)^{-1}\frac{h}{2}\frac{\partial \mathbf{g}_{s,f}}{\partial \boldsymbol{\Phi}_f}, & \left(\mathbf{I}-\frac{h}{2}\frac{\partial \boldsymbol{S}_{f,f}}{\partial \boldsymbol{\Phi}_f}\right)^{-1}\frac{h}{2}\frac{\partial\left(\boldsymbol{S}_{f,f}+\mathbf{g}_{s,f}\right)}{\partial \boldsymbol{\Phi}_s} \\ \frac{h^2}{4}\frac{\partial \boldsymbol{S}_{f,s}}{\partial \boldsymbol{\Phi}_f}\left(\mathbf{I}-\frac{h}{2}\frac{\partial \boldsymbol{S}_{f,f}}{\partial \boldsymbol{\Phi}_f}\right)^{-1}\frac{\partial \mathbf{g}_{s,f}}{\partial \boldsymbol{\Phi}_f}+\frac{h}{2}\frac{\partial \mathbf{g}_{s,s}}{\partial \boldsymbol{\Phi}_f}, & \frac{h^2}{4}\frac{\partial \boldsymbol{S}_{f,s}}{\partial \boldsymbol{\Phi}_f}\left(\mathbf{I}-\frac{h}{2}\frac{\partial \boldsymbol{S}_{f,f}}{\partial \boldsymbol{\Phi}_f}\right)^{-1}\frac{\partial\left(\boldsymbol{S}_{f,f}+\mathbf{g}_{s,f}\right)}{\partial \boldsymbol{\Phi}_s}+\frac{h}{2}\frac{\partial\left(\boldsymbol{S}_{f,s}+\mathbf{g}_{s,s}\right)}{\partial \boldsymbol{\Phi}_s} \end{bmatrix} \quad (8)$$

where the subscripts "*f*" and "*s*" indicate the sub-blocks in a rate vector corresponding to the fast and slow variables, respectively. Considering that $\partial \boldsymbol{S}_f/\partial \boldsymbol{\Phi}_f = \boldsymbol{O}(1/\tau)$, where τ is the fastest chemical timescale and $\tau < h$, and $\partial \mathbf{g}_s/\partial \boldsymbol{\Phi}_f,\ \partial \boldsymbol{S}_f/\partial \boldsymbol{\Phi}_s, \partial \mathbf{g}_s/\partial \boldsymbol{\Phi}_s = \boldsymbol{O}(1)$, the orders of different blocks of $\boldsymbol{A}$ can be expressed as

$$\boldsymbol{A} = \begin{bmatrix} \boldsymbol{O}(\tau) & \boldsymbol{O}(\tau) \\ \boldsymbol{O}(h) & \boldsymbol{O}(h) \end{bmatrix} = \boldsymbol{O}(h) \quad (9)$$

which indicates that the spectral radius of $\boldsymbol{A}$ is $\boldsymbol{O}(h)$, and the iterations converges quickly when the integration time step is small.

3. Results and Discussion

3.1 Convergence test of AHI2 for a toy problem

To demonstrate that the convergence rate in the iterations of AHI2 is $\boldsymbol{O}(h)$, the toy problem in [21] is first used:

$$A \xrightarrow{k_1} R \quad (R1)$$

$$R \xrightarrow{k_2} C \quad (R2)$$

$$A + \alpha R \xrightarrow{k_3} B + \alpha R \quad (R3)$$

where k_1, k_2 and k_3 are the rate coefficients for *R1*, *R2* and *R3*, respectively. Species *A* is a reactant, *B* is a product, *C* is an intermediate species which is not of direct importance to *A* and *B*, and *R* is a radical that controls the important reaction *R3* for product formation. The parameter α controls the overall reaction order and nonlinearity of *R3*.

The transport term of *R* is set to be a constant *d* for simplicity, and for other species, the transport terms are set to be zero. The dependent variables and source terms in Eq. (1) can be thereby expressed as:

$$\boldsymbol{\Phi} = [A, B, C, R]^T$$
$$\boldsymbol{S} = [-k_1 A - k_3 A R^\alpha, k_3 A R^\alpha, k_2 R, k_1 A - k_2 R]$$
$$\boldsymbol{M} = [0, 0, 0, d]$$

The initial conditions are:

$$A = 1, B = C = R = 0 \text{ at } t = 0.$$

The reaction rate coefficient k_2 is chosen to be much larger than k_1, i.e. $k_2 \gg k_1$, such that *R* is a quasi-steady state (QSS) species after an initial transient period and can be approximated as:

$$R \approx \frac{k_1 A + d}{k_2} \quad (10)$$

In the present study, the parameters are chosen as: $k_1 = 1$, $k_2 = \tau^{-1}$, $k_3 = \tau^{-\alpha}$, $d = 1$. Note that k_3 is selected such that the rate of reaction *R3*, $\Omega_3 = k_3 A R^{\alpha} = O(1)$. The timescale of *R* can be defined as $\tau = 1/k_2$, and the timescales of other species are $O(1)$. It is expected that the toy problem can be implicitly integrated with a time step *h* between τ and 1. Based on such selected integration time steps, *R* is the only fast species, and *R2* and *R3* are fast reactions. It is further noted that species *A* and *R* can be solved as a self-consistent system with source terms as

$$S_A = -k_3 A R^{\alpha}, \mathrm{g}_A = -k_1 A$$
$$S_R = -k_2 R, \mathrm{g}_R = k_1 A + d$$

The iteration matrix can be written as

$$\mathbf{A} = \begin{bmatrix} 0 & \left(1 + \frac{h}{2}\frac{1}{\tau}\right)^{-1} \frac{h}{2} k_1 \\ 0 & \frac{h^2}{4}(-k_3 \alpha A R^{\alpha-1}) \left(1 + \frac{h}{2}\frac{1}{\tau}\right)^{-1} k_1 + \frac{h}{2}(-k_3 R^{\alpha} - k_1) \end{bmatrix} = \begin{bmatrix} 0 & O(\tau) \\ 0 & O(h) \end{bmatrix} \tag{11}$$

and the spectral radius of $\mathbf{A}$ is $O(h)$, being consistent to Eq. (9). The relative errors in the midpoint rates $\boldsymbol{k}^{\frac{1}{2}}$ for species *k* and a variable Φ are defined as

$$\varepsilon_k^m = \frac{\left| k_k^{\frac{1}{2},m} - k_k^{\frac{1}{2},m+1} \right|}{\left| k_k^{\frac{1}{2},m} + k_k^{\frac{1}{2},m+1} \right|}, \varepsilon_{\Phi} = \frac{|\Phi - \Phi^E|}{|\Phi + \Phi^E|} \tag{12}$$

where the superscript E indicates the accurate solution. Figure 1 shows the relative errors at different iterations within a single integration step, starting from the accurate solution at $A = 0.5$. It is seen that the relative errors decrease with a slope of *h* on the log plot, as predicted by Eq. (11). Two iterations are needed for *A* and three needed for *R* to achieve second order accuracy. Figure 2 further shows the local relative errors in the concentrations of *A* and *R* incurred by one integration time step started at $A = 0.5$. It is seen in Fig. 2a that, with two iterations per integration time step, the single-step relative errors in *A* and *B* are both $O(h^3)$, while *R* needs another iteration to achieve second-order accuracy as shown in Fig. 2b.

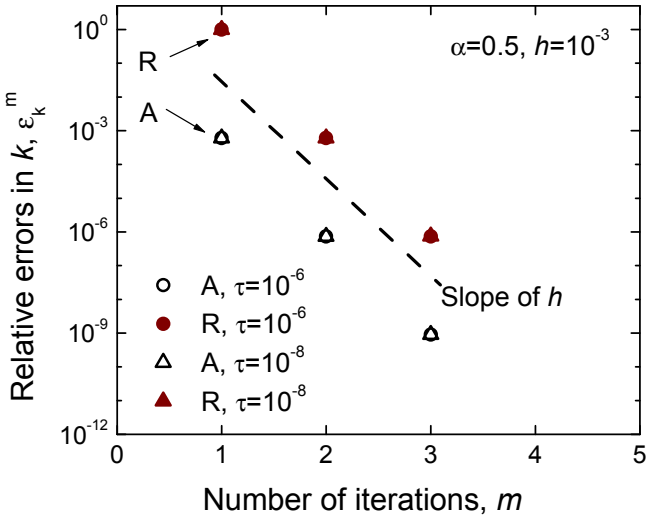

Figure 1. Relative errors in rates $\boldsymbol{k}$ between two successive iterations with respect to the number of iterations for $\alpha = 0.5$, $h = 10^{-3}$ in the toy problem. Open symbols: relative errors in the rate

of A, closed symbols: relative errors in the rate of R. Circles: $\tau = 10^{-6}$, triangles: $\tau = 10^{-8}$. Dashed line: trend line with a slope of h.

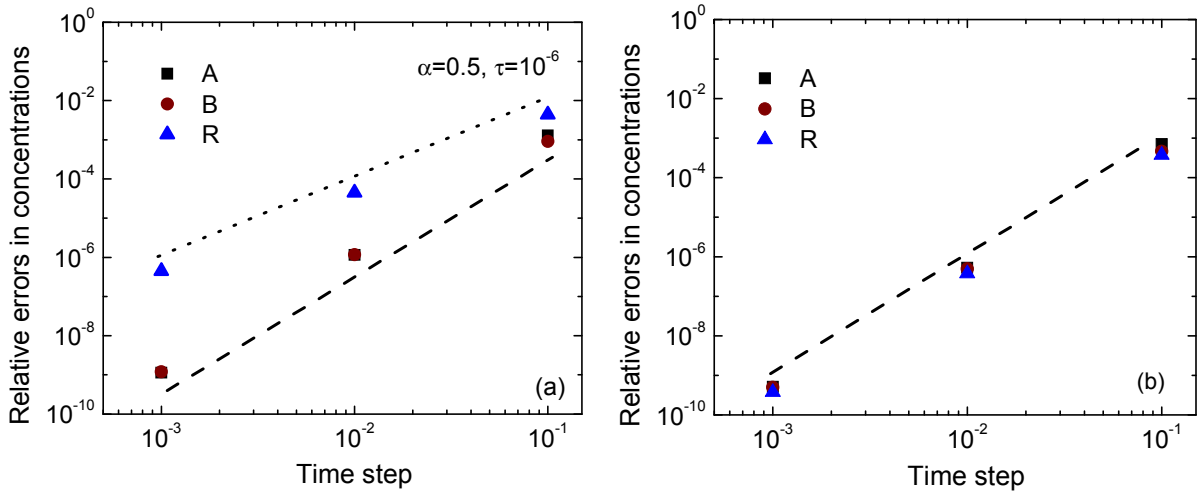

Figure 2. Local relative errors as function of integration time step size in species concentrations with (a) two iterations and (b) three iterations per integration step. Dotted line: trend line with slope of 2. Dashed line: trend line with a slope of 3.

3.2 Comparison with the Strang splitting scheme

Figure 3 shows the relative error in the concentration of species B measured at $A = 0.5$ with different splitting time step Δt and integration time step h, respectively. It is seen that the Strang splitting scheme starts to show second-order behavior only when the splitting time step is close to and smaller than τ. In comparison, AHI1 and AHI2 show expected orders of accuracy across the entire range of integration time steps, and the accuracy was improved by many orders of magnitudes compared with the splitting scheme.

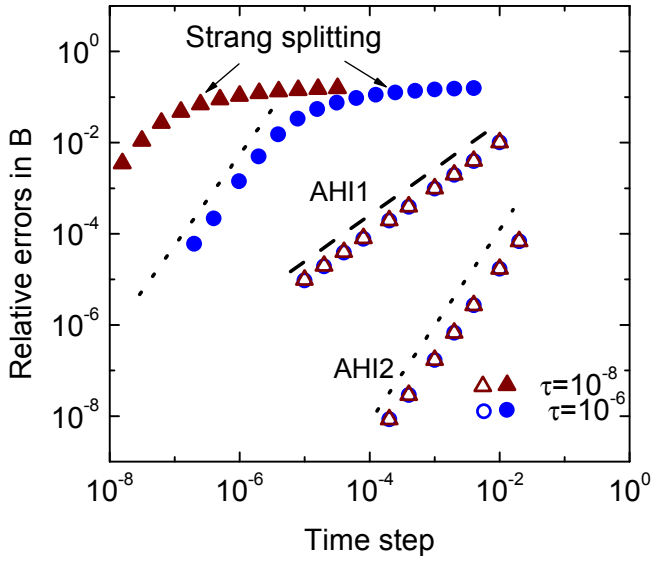

Figure 3. Relative errors in B for the toy problem with $\alpha = 0.5$, measured at the time when A=0.5, as function of the time step size, for two different timescales of R. Triangles: $\tau = 10^{-8}$. Circles: $\tau = 10^{-6}$. Dashed and dotted lines: slope of 1 and 2, respectively.

3.3 Performance of AHI2 with detailed chemistry

The accuracy of AHI2 is further tested in the auto-ignition of H_2/air under constant pressure using detailed chemistry [29]. Note that no transport term is involved. Figure 4 shows the species mass fractions, temperature and relative errors of AHI2 for the auto-ignition case. Figure 4a shows that the solution from AHI2 agrees with that from DASAC using relative error tolerance of 10^{-8} and absolutely error tolerance of 10^{-20}. Taking the solution from DASAC as an accurate solution, Fig. 4b shows the relative errors in AHI1 and AHI2, respectively. It is seen that the errors from AHI2 is substantially reduced in comparison with AHI1.

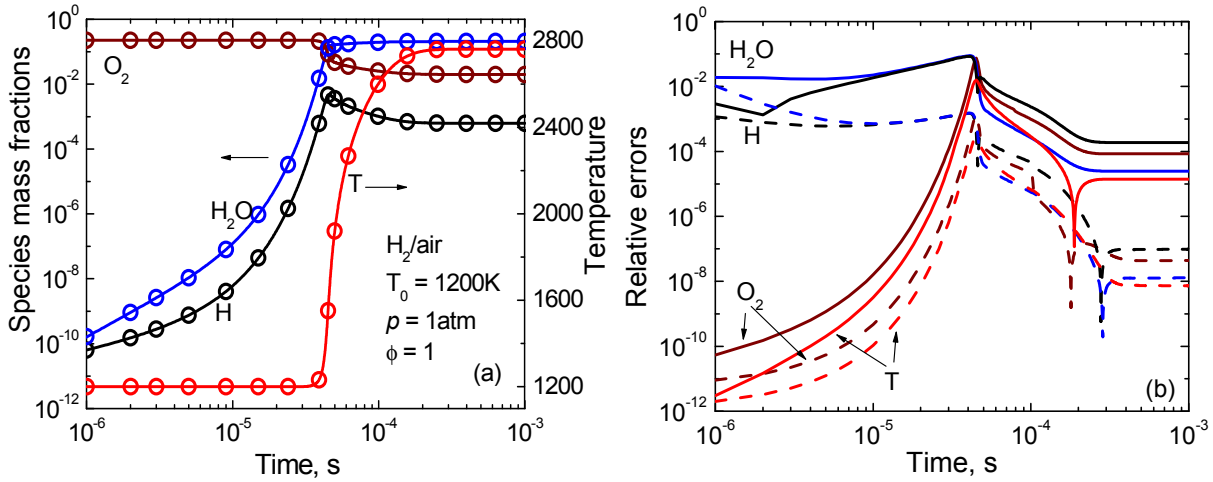

Figure 4. (a) Profiles of species mass fraction and temperature in constant-pressure auto-ignition of stoichiometric hydrogen/air, calculated AHI2 with $h = 10^{-7}s$ (symbols), in comparison with an accurate solution obtained using DASAC (solid lines). (b) Relative errors in species concentrations and temperature in AHI1 (solid lines) and AHI2 (dashed lines).

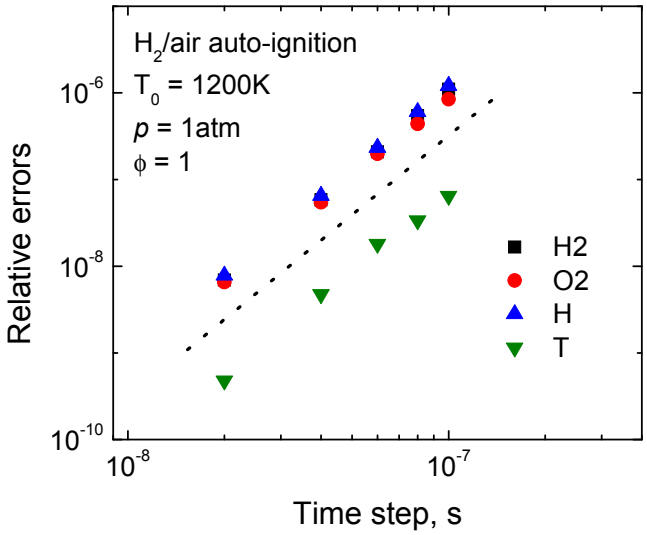

Figure 5. Local relative errors in different variables of AHI2 as function of integration time step size for constant-pressure auto-ignition of stoichiometric hydrogen/air. Dotted line: slope of 3.

To further validate the order of accuracy of AHI2 for the auto-ignition case, a single integration step is invoked at the inflection point on the temperature profile, which typically

defines the ignition state. The relative errors in different variables incurred in the integration step are plotted in Fig. 5. A linear dependence with slope of 3 can be clearly seen, and the overall second-order accuracy is confirmed.

The efficiency of AHI2 is then tested in constant-pressure auto-ignition and unsteady PSR, which involves a homogeneous mixing term, using different reaction models, including a 9 species detailed model for hydrogen/air [29], a 32-species skeletal model for ethylene/air [30], and the 111-species detailed USC-Mech II reaction model [31] using methane as fuel.

The auto-ignition cases are initialized with stoichiometric fuel/air mixture at p = 1 atm, and $T_0 = 1200\,K$. The unsteady PSR cases are initialized with the steady state solution with temperature perturbed by +10 K such that the reactor relaxes toward the steady state solution during the time integration. The inlet streams of the PSRs consist of fresh stoichiometric fuel/air mixtures at $T_{in} = 300\,K$, and the residence time is set to τ_{res} = 1 ms. All the cases for auto-ignition and unsteady PSR are integrated from $t = 0\ to\ 0.05\,s$ with a fixed time step size of $h = 10^{-7}$s. All the systems have mostly reached steady state at the end of the integration. For the auto-ignition cases, the total CPU time of AHI is normalized by the cost with all the species and reactions being solved implicitly. For the unsteady PSR cases, the CPU time is normalized by that of Strang splitting scheme, where the chemistry sub-step is integrated using VODE with analytic Jacobian, and the transport is solved explicitly. Figure 6 shows the corresponding speedup using AHI1 and AHI2, respectively. Note that the time saving for the auto-ignition cases are attributed to the reduced number of variables to be solved implicitly. It is seen that the time saving increases with the size of reaction models, indicating a larger extent of reduction in the number of fast species for larger reaction models.

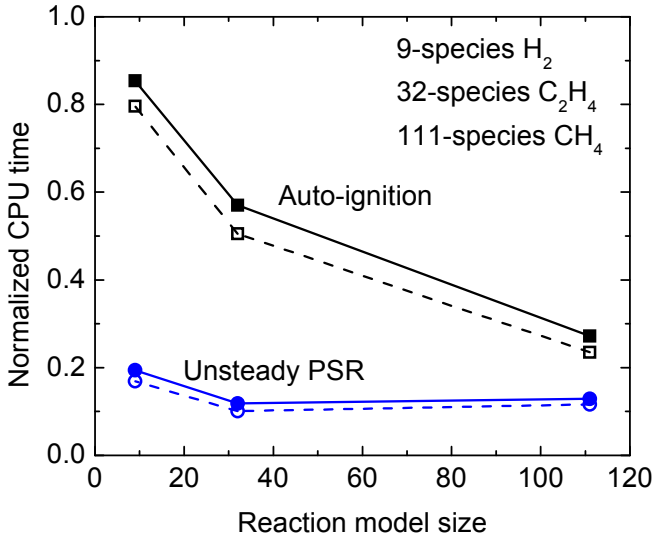

Figure 6. CPU time for the integration of constant-pressure auto-ignition normalized by that of fully implicit integration, and for unsteady PSR normalized by that of the Strang splitting scheme using VODE with analytic Jacobian for chemistry integration, for stoichiometric different fuel/air mixtures at atmospheric pressure, inlet temperature of 300 K, and residence time of 1 ms. Solid lines: AHI1, dashed lines: AHI2.

Significantly larger time savings are observed for the unsteady PSR cases. The speedup factors of 5~10, compared with the splitting scheme, are primarily attributed to the effect of transport term on fast chemistry modes, as discussed in the previous AHI study [21]. As a result,

the splitting schemes requires multiple sub-steps in each chemical sub-step to exhaust the activated fast chemical modes, while such an issue is not present in the AHI schemes. As such, the AHI methods can be substantially more efficient than the splitting schemes even if adaptive fast chemistry is not involved, i.e. all the species and reactions are treated implicitly. It is further noted that the efficiencies of AHI and AHI2 only differ slightly for the auto-ignition and unsteady PSR cases. This is because the Jacobian of the fast chemistry doesn't need to be updated during the iterative procedure, such that the overhead to achieve the second order accuracy is rather small.

4. Conclusions

A second-order adaptive hybrid scheme is developed for stiff chemistry integration and validated. The convergence rate of the iterative procedure to achieve second order accuracy is analyzed based on the spectral radius of the iterative matrix. It is shown that only about three iterations are needed to achieve the expected accuracy for both the toy problem and detailed chemistry. Error control of AHI1 and AHI2 is compared with the Strang splitting scheme using the toy problem, and the AHI schemes show dramatically improved accuracy.

The accuracy and efficiency of AHI2 are further studied with detailed chemistry, and second-order accuracy is verified in constant-pressure auto-ignition with detailed chemistry for H_2/air, and AHI2 achieves substantially smaller relative errors in the auto-ignition case. Compared with the fully implicit scheme, AHI schemes reduce computation primarily through the reduction in the number of variables to be solved implicitly, and such time saving increases with the size of the reaction models, reaching ~80% for the 111-species detailed USC-Mech II. For the unsteady PSR cases involving a transport term, the AHI schemes achieved significant speedup compared to the splitting scheme, due to need to exhaust the reactive fast chemical modes in each chemistry sub-step of the splitting schemes. Overall, the AHI schemes achieved speedup factors of 5-10 compared with the splitting schemes in the unsteady PSR cases. In term of accuracy, AHI2 is shown to be significantly more accurate than AHI1, while the computational cost is only slightly increased.

5. Acknowledgements

This work is supported by the Air Force Office of Scientific Research under Grant FA9550-13-1-0057. The work by Z. Ren is supported by National Natural Science Foundation of China (51476087).

6. References

[1] T. F. Lu, C. K. Law, Prog. Energy Combust. Sci. 35 (2) (2009) 192-215.
[2] P. Brown, G. Byrne, A. Hindmarsh, SIAM Journal on Scientific and Statistical Computing 10 (5) (1989) 1038-1051.
[3] M. Caracotsios, W. E. Stewart, Comput. Chem. Eng. 19 (9) (1995) 1019-1030.
[4] G. Marchuk, On the theory of the splitting-up method, in: Proceedings of the 2nd Symposium on Numerical Solution of Partial Differential Equations, SVNSPADE, 1970; pp 469-500.
[5] N. N. Yanenko, in: The method of fractional steps, Springer-Verlag: New York, 1971.
[6] O. M. Knio, H. N. Najm, P. S. Wyckoff, J. Comput. Phys. 154 (2) (1999) 428-467.
[7] B. Sportisse, J. Comput. Phys. 161 (1) (2000) 140-168.
[8] D. A. Schwer, P. Lu, W. H. Green, V. Semiao, Combust. Theory Model. 7 (2) (2003) 383-399.
[9] D. L. Ropp, J. N. Shadid, C. C. Ober, J. Comput. Phys. 194 (2) (2004) 544-574.
[10] M. A. Singer, S. B. Pope, H. N. Najm, Combust. Theory Model. 10 (2) (2006) 199-217.
[11] G. Strang, SIAM Journal on Numerical Analysis 5 (3) (1968) 506-517.

[12] Z. Ren, S. B. Pope, J. Comput. Phys. 227 (17) (2008) 8165-8176.
[13] M. Duarte, M. Massot, S. Descombes, C. Tenaud, T. Dumont, V. Louvet, F. Laurent, SIAM J. Sci. Comput. 34 (1) (2012) A76-A104.
[14] Z. Ren, C. Xu, T. Lu, M. A. Singer, J. Comput. Phys. 263 (2014) 19-36.
[15] U. M. Ascher, S. J. Ruuth, R. J. Spiteri, Appl. Numer. Math. 25 (2–3) (1997) 151-167.
[16] U. M. Ascher, S. J. Ruuth, B. T. R. Wetton, SIAM Journal on Numerical Analysis 32 (3) (1995) 797-823.
[17] S. Ruuth, J. Math. Biol. 34 (2) (1995) 148-176.
[18] E. Lindblad, D. M. Valiev, B. Müller, J. Rantakokko, P. Lütstedt, M. A. Liberman, in: Shock Waves, K. Hannemann; F. Seiler, (Eds.) Springer Berlin Heidelberg: 2009; pp 299-304.
[19] J. G. Verwer, B. P. Sommeijer, SIAM J. Sci. Comput. 25 (5) (2004) 1824-1835.
[20] J. J. Yoh, X. Zhong, AIAA Journal 42 (8) (2004) 1593-1600.
[21] Y. Gao, Y. Liu, Z. Ren, T. Lu, Combust. Flame 162 (2) (2015) 287-295.
[22] R. Speth, W. Green, S. MacNamara, G. Strang, SIAM Journal on Numerical Analysis 51 (6) (2013) 3084-3105.
[23] M. J. McNenly, R. A. Whitesides, D. L. Flowers, Proc. Combust. Inst. 35 (1) (2015) 581-587.
[24] F. Perini, E. Galligani, R. D. Reitz, Combust. Flame 161 (5) (2014) 1180-1195.
[25] F. Perini, E. Galligani, G. Cantore, R. Reitz, SAE Technical Papers 8 (2012).
[26] F. Perini, E. Galligani, R. D. Reitz, Energy Fuels 26 (8) (2012) 4804-4822.
[27] D. A. Schwer, J. E. Tolsma, W. H. Green, P. I. Barton, Combust. Flame 128 (3) (2002) 270-291.
[28] S. H. Lam, Combust. Flame 160 (12) (2013) 2707-2711.
[29] J. Li, Z. W. Zhao, A. Kazakov, F. L. Dryer, Int. J. Chem. Kinet. 36 (10) (2004) 566-575.
[30] Z. Luo, C. S. Yoo, E. S. Richardson, J. H. Chen, C. K. Law, T. Lu, Combust. Flame 159 (1) (2011) 265-274.
[31] H. Wang, X. You, A. Joshi, S. Davis, A. Laskin, F. Egolfopoulos, C. Law USC Mech Version II. High-Temperature Combustion Reaction Model of H2/CO/C1-C4 Compounds. http://ignis.usc.edu/USC_Mech_II.htm